





Geochemical characterization of Lithium-bearing brines from Guaranda, Ecuador

John Manrique-Carreño^{1*} ; Érika Martínez-Villa¹ 
Érika Calderón-Maza¹ ; Galo Guamán-Jaramillo¹ 

¹Departamento de Geociencias, Universidad Técnica Particular de Loja, San Cayetano Alto, Loja, Ecuador. (*) jmanrique@utpl.edu.ec, emmartinez7@utpl.edu.ec, elcalderon@utpl.edu.ec, gaguaman2@utpl.edu.ec

Abstract

Lithium is considered a critical metal for its technological use. It was proposed to carry out the geochemical prospecting study in favorable environments to host possible lithium mineralization, in specific sectors of Ecuador. This would be important, as no anomalies of economic interest have been discovered to date. The content of Li in solid samples and hydrothermal waters in brines in the Guaranda sector, Bolívar province, was evaluated. Likewise, a mineralogical analysis of the solid samples and a multivariate statistical analysis of the data was carried out. The values of sub-anomalies of Li (median 222.46 mgL⁻¹ in brines and Li in solids from Guaranda (median 201.5 ppm), may be comparable to exploitable Li deposits worldwide, which is interesting for its possible economic use. Based on the multivariate statistical analysis, chemical and mineralogical results, Li is associated with Be, and Na mainly in the solids analyzed, this is evidenced by the detection of saponite and fluoroferroleakeite. The chemical composition of the sampled waters could be the result of several processes that include: the dissolution of minerals by water-rock interaction, hydrothermal fluids related to active volcanism and/or recharge by meteoric waters.

Keywords: Lithium; Brines; Hydrogeochemistry; Salts; Guaranda.

Caracterización geoquímica de salmueras con litio de Guaranda, Ecuador

Resumen

El litio es considerado un metal crítico por su uso tecnológico. Por esta razón se propuso realizar el estudio de prospección geoquímica en ambientes favorables para albergar posibles mineralizaciones de litio, en sectores específicos del Ecuador. Esto es importante, ya que no se han descubierto anomalías de interés económico hasta la fecha. Se evaluó el contenido de Li en muestras sólidas y aguas hidrotermales en salmueras en el sector Guaranda, provincia de Bolívar. Asimismo, se realizó un análisis mineralógico de las muestras sólidas y un análisis estadístico multivariado de los datos. Los valores de sub-anomalías de Li (222,46 mgL⁻¹ mediana) en salmueras y Li en sólidos de Guaranda (201,5 ppm mediana), pueden ser comparables a depósitos de Li explotables a nivel mundial, lo cual es interesante por su posible aprovechamiento económico. Con base en el análisis estadístico multivariado y en los resultados químicos y mineralógicos, el Li se encuentra asociado con Be, Na principalmente, en los sólidos analizados, esto se evidencia en la detección de saponita y fluoroferroleakeíta. La composición química de las aguas muestreadas podría ser el resultado de varios procesos que incluyen, disolución de minerales por interacción agua-roca, fluidos hidrotermales relacionados con vulcanismo activo y/o recarga por aguas meteóricas.

Palabras clave: Litio; Salmueras; Hidrogeoquímica; Sales; Guaranda.

How to cite: Manrique-Carreño, J.; Martínez-Villa, E.; Calderón-Maza, E.; Guamán-Jaramillo, G. (2023). Geochemical characterization of Lithium-bearing brines from Guaranda, Ecuador. *Boletín de Geología*, 45(2), 79-92. <https://doi.org/10.18273/revbol.v45n2-2023005>

Introduction

Lithium (Li) is an alkaline element, of a lithophilic geochemical nature, that is, it has an affinity for silicates and oxides in rocks. The physical and chemical properties of lithium and its compounds allow them to be used in various industries: glass and ceramic manufacturing, lithium ion batteries (LIBs), lubricants, air treatment, steel industry, production of pharmaceuticals and polymers, primary aluminum production, among other uses (Changes and Swiatowska, 2015). World lithium reserves are 22 million tons, of which Chile has 41%, Australia 25% and, Argentina 10% (USGS, 2022).

The crustal abundance of Li is low, the Clarke in the crust is 20 ppm, and varies according to the type of rock and reservoir, the mean values of various lithologies and aquatic regimes are given as follows: basic rocks 17 ppm Li, intermediate rocks 20 ppm Li, syenites 28 ppm Li, granites 40 ppm Li, shales 66 ppm Li, sandstones 15 ppm Li, carbonate rocks 5 ppm Li, river water 3 mgL⁻¹ Li, sea water 180 µgL⁻¹ Li (Dill, 2010).

Lithium is found in three main types of deposits: 1) Li-rich pegmatite magmatic deposits containing spodumene (LiAlSi₂O₆) and rhyolitic tuffs containing Li, F and Be. 2) continental brines, and 3) hydrothermally altered clays, with hectorite (Na_{0.3}(Mg,Li)₃Si₄O₁₀(OH)₂) (Webmineral, 2022) formed by hydrothermal alteration of volcanoclastic rocks (Munk *et al.*, 2016). Other secondary sources of lithium include: salt flats, and formational waters of oil fields, (Dill, 2010; Pohl, 2011; USGS, 2022).

It was proposed to carry out the geochemical prospecting study in favorable environments to host possible lithium mineralization, in a specific sector of Ecuador. Detecting any anomaly or occurrence would be of great importance for the country, since no anomalies of economic interest have been discovered (Inguaggiato *et al.*, 2010; Gonzaga *et al.*, 2017). In this case, a sampling of evaporite salts was carried out in Salinas de Guaranda, Bolívar province, in which a total of 8 water samples (brines) and 8 solid samples (salts and crusts).

The study area

Location

The Salinas de Guaranda sector is located in the Bolívar province, Guaranda canton, Salinas parish, northeast of the city of Guaranda (Ecuador) (Figure 1), at an altitude of 3,550 meters above sea level. It takes

its name from the saltwater mines that can be found when crossing the river that runs through it and that bears the same name. Until the years 1960-1970, the exploitation of these salt mines was the main economic activity of the inhabitants of that time, complemented by agricultural work in small plots and an incipient livestock activity until the end of the 60s. Some studies have detected high Li values of 10.808 meq/L (Inguaggiato *et al.*, 2010) to the average Li in seawater 0.18 mgL⁻¹ (180 µgL⁻¹, 0.026 meq/L) (Li, 1982).

Geological setting

The Salinas sector is located on the western flanks of the Western Cordillera (Figure 2), located in rocks of the Zumbagua Group, consisting of poorly classified coarse-grained sandstones and unclassified debritic breccias and matrix supported by forming layers of several meters thick, acidic to intermediate tuffs, tuff sandstones and locally, in the Salinas area horizontal gaps interpreted as laharitic units that form an elongated body oriented from north to south are also visible. The sandstones are rich in lithics and/or crystals (quartz-feldspar-amphibole); clasts in coarse sandstones, breccias, and lahars are almost exclusively volcanic material. Zircon fission trace ages of tuff and tuff sandstones indicate Middle to Late Miocene (16.8-7.9 Ma) (BGS-CODIGEM, 1997).

The source of saline water that arises in these rocks, forms calcareous and saline concretions on the surface that form a karst landscape with multiple sources no larger than 1m², which constitute exit points (upwellings) of gas and water that carry ions and minerals through a process of dissolution (and also mechanical erosion) than can be produced by a system of interconnected underground conduits (Andreu *et al.*, 2016).

To the west is the Arrayanes Unit (EAR) from the Late Eocene, made up of volcanic rocks and volcano sediments with andesite-basaltic lavas. This unit is superimposed on the Macuchi Unit (PcEM) from the Early to Middle Eocene, which comprises volcanic sandstones, breccias, tuffs, gabbros diabases, subporphytic basalts, padded lavas and few calcarenites. The unit shows definitive characteristics of an insular arch and includes basalts to subalkaline basaltic andesites of tholeiitic affinity to chalcoalkaline with geochemical characteristics related to subduction. All these sequences are intruded by extensive plutons of medium to coarse-grained tonalites and granodiorites with ages of 35 to 10 Ma (BGS-CODIGEM, 1997).

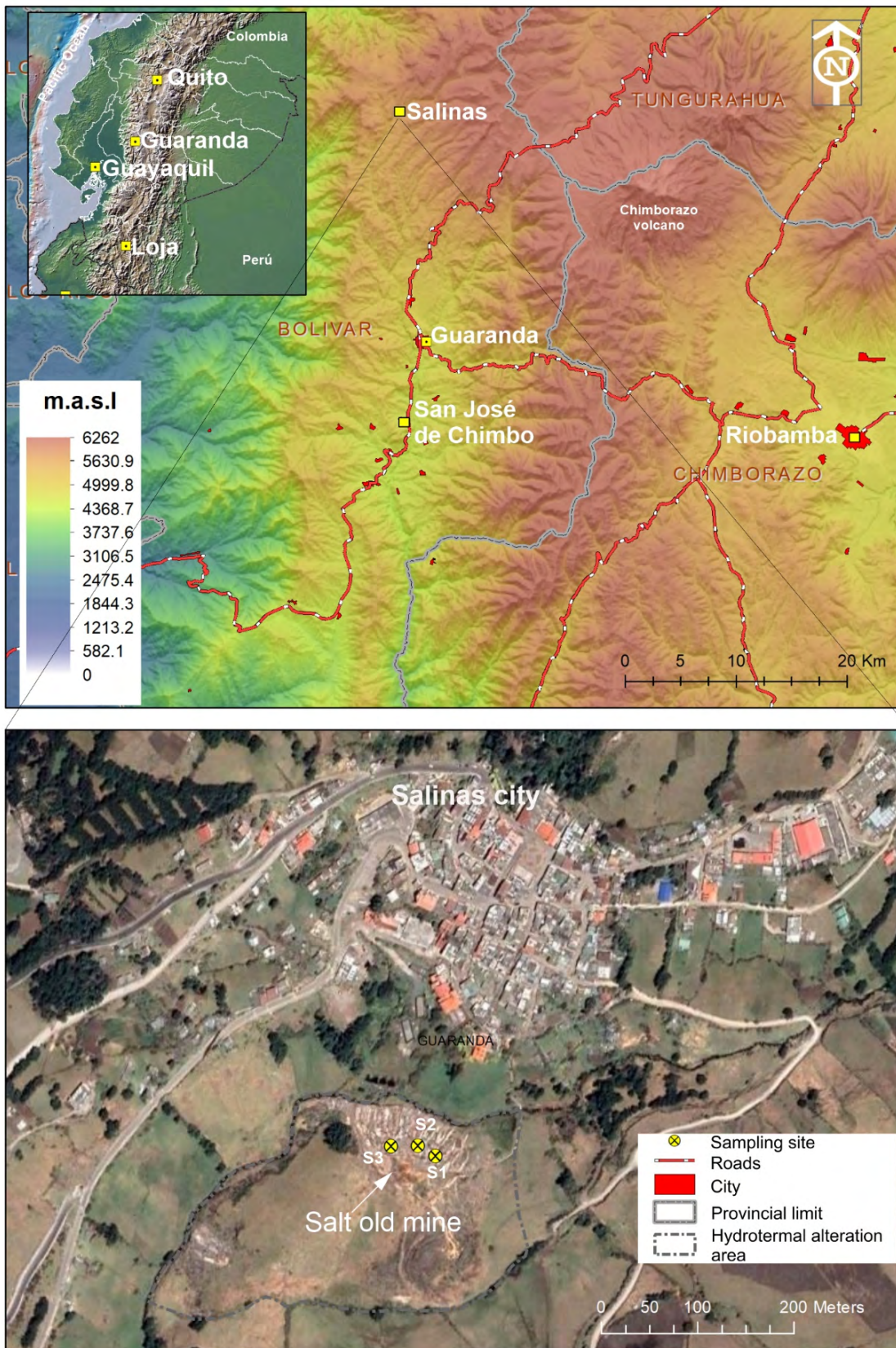


Figure 1. Salinas de Guaranda location (MDT obtained of SRTM and Google Earth Image).

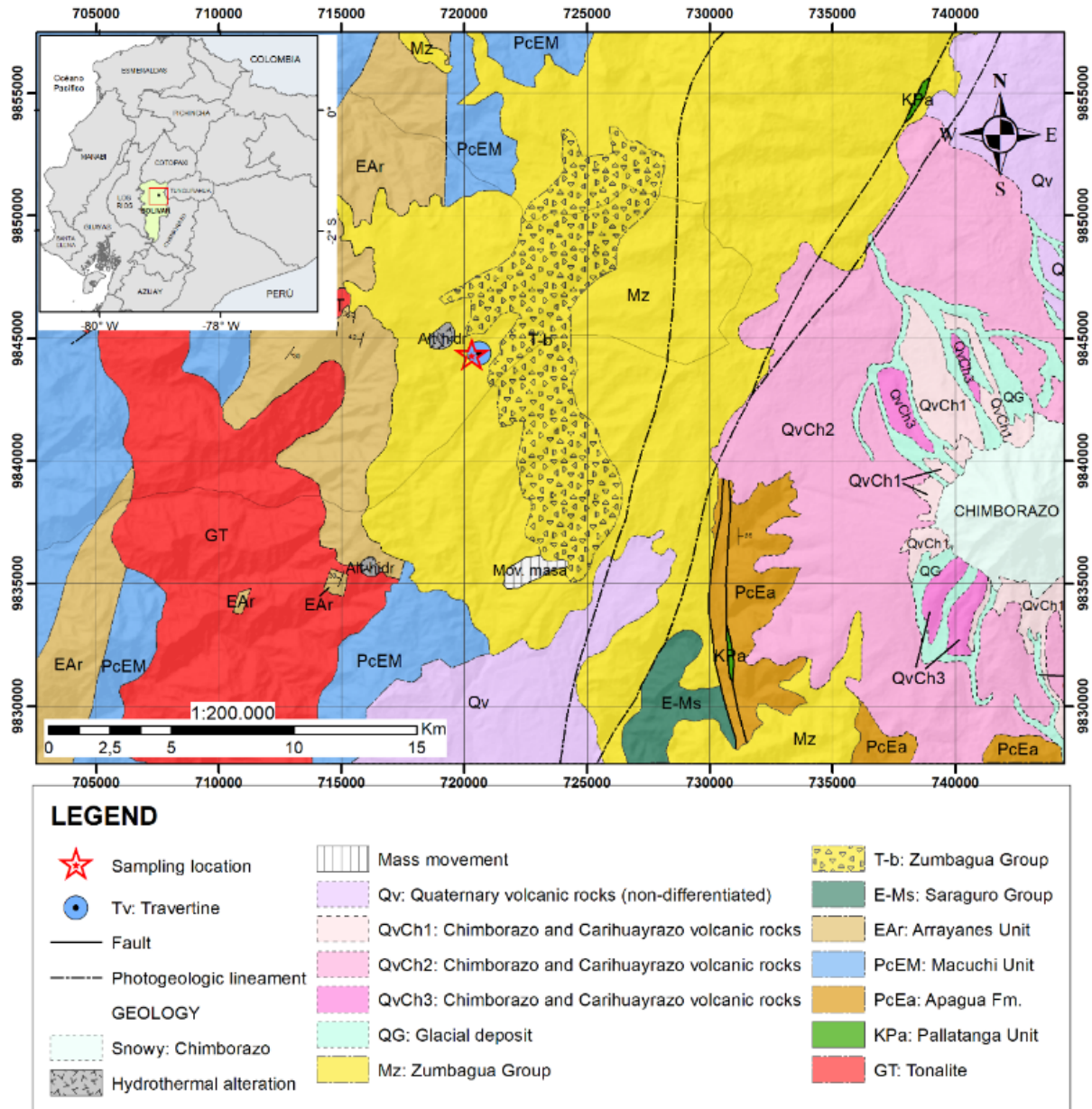


Figure 2. Geology setting of Guaranda (BGS-CODIGEM, 1997).

To the east, the volcanic rocks of the Chimborazo and Carihuayrazo Volcanoes (QvCh 1-3) predominate, including lavas, pyroclastic flows, lahars, debris avalanches and ash deposits. The lavas of Carihuayrazo and the oldest of Chimborazo (QvCh 1) are phryic andesites with pyroxene; the youngest Chimborazo lavas (QvCh 2), which are confined to the southeast flanks, are pyroxene andesites and pyroxene vesicular dacites. The youngest products (QvCh 3) are found along the western flanks and include lahars, debris avalanches, lavas, and coarse-grained tuffs, pumaceous,

of general andesitic to dacitic composition. Some Undifferentiated Quaternary volcanoes (QV) include tuffs, breccias, agglomerates and andesitic lavas from the Pleistocene of older volcanic centers such as Chimborazo and Carihuayrazo. Also included in this general unit are the Guaranda Volcanoes, a series of andesitic tuffs and porphyritic andesites from the Pleistocene. The youngest deposit in this unit is an unstratified, partially consolidated volcanic ash from the Late Pleistocene to Holocene Cangahua Unit (BGS-CODIGEM, 1997).

Methods

The water samples were taken from the three saline upwelling pools (hydrothermal brines) (review supplemental material for coordinates and lab results). A volume of 200 mL to 500 mL was collected per sampling point and some physicochemical parameters such as pH and, temperature were measured (*in situ*). Then each sample was acidified with 1.5 mL of concentrated nitric acid (HNO_3) (only for the case of cation analysis) and they were refrigerated until their analysis in the laboratory. To see the complementary data, review [Supplementary Table 1](#).

In the laboratory, the water samples were filtered by 45-micron filter paper and analyzed using Optical Emission Spectrometry with Inductive Coupling Plasma (ICP-OES) Perkin Elmer Optima 800 DV model, in the Analytical Geochemistry Laboratory of the Geosciences Department, Universidad Técnica Particular de Loja (UTPL), after calibration with certified multielement standards. In this analysis, the concentration of major, minor and trace elements was obtained: Ca, K, Mg, Na, Zn, Pb, Cd, Ba, Fe, Mn, Li, Rb, Be, and Sr. The anion analyzes (Cl^- , CO_3^{2-} , HCO_3^- , SO_4^{2-}) were carried out by titration, except for sulfate (SO_4^{2-}) which was analyzed by UV/VIS spectrophotometry.

Solid samples were collected from the evaporation and salt crystallization around the pools (review supplemental material for coordinates and lab results),

as well as from a calcareous crust that surrounds the hydrothermal brine upwelling pools ([Figure 3](#)), approximately 200 g of fresh material per sample. The samples were dried at 105°C for 24 hours in the oven, then they were cut, crushed and pulverized. The chemical analyses of two replicas were made in Actlabs, Canada, and carried out using the analytical package: Code 8-Li (Sodium Peroxide Fusion just for Li) (to see the complementary data, review [Supplementary Table 2](#)). All samples were analyzed using an XRF spectrometer Bruker S1 Turbo and, Optical Emission Spectrometry with Inductive Coupling Plasma (ICP-OES) at UTPL, detecting the following elements (with its detection limits or lower limits): Si (0.01 wt%), Al (0.01 wt%), Fe (0.01 wt%), Mg (0.01 wt%), Ca (0.01 wt%), Na (0.01 wt%), K (0.01 wt%), P (0.01 wt%), S (0.01 wt%), Ba (0.1 ppm), Be (0.1 ppm), Mn (0.1 ppm), Li (0.1 ppm), Rb (0.1 ppm) and, Sr (0.1 ppm).

X-ray diffraction (XRD) analyses were performed on pulverized rock samples using a Bruker, model D8 Advance diffractometer, in the XRD laboratory of the Department of Chemistry and Exact Sciences of UTPL, Ecuador, with the following specifications: Cu X-ray generator tube, K-Alpha 1.5418 (Å), SSD 160 detector, with a set of 40 kV and 25 mA, with a linear count of up to 2,106 cps and step times of 0.5. The software used for the processing were: EVA Diffrac Plus and TOPAS, using the Structure D8 and COD references files (databases). Phase quantification was made using the Rietveld Method with TOPAS software.



Figure 3. Guaranda location, hydrothermal brine upwelling pools.

Results

Li-bearing brines of the Guaranda

The statistical treatments of the chemical data (cations and anions) of the Li-bearing brine of Guaranda are given in Table 1. Contents of Zn, Cd and Fe reached sub-anomalies values (median + 2 standard deviation), whereas sub-anomalies or anomalies of other trace elements, such as Pb, Ba, Mn, Li, Rb, Se, Be and Sr, were not detected.

Regarding the physicochemical parameters measured *in situ*, the range of pH values was from 4 to 5 and the surface temperature of the water was from 13 to 17°C, which may be due to the ambient temperature of the sampling site (Inguaggiato *et al.*, 2010).

In the Piper diagram (Figure 4), in the triangle of the anions, it can be observed that all the samples are grouped at the end of the chloride face, indicating a total predominance of the chloride ion (close to 100). The same behavior can be observed in the triangle of cations, where all the samples are grouped at one end of the sodium face, indicating the absolute predominance of this ion. From this it is concluded that all the samples in the Salinas de Guaranda sector are of the sodium chloride type.

The Schöeller-Berkaloff diagram (Figure 5) indicate that all the brine samples have a similar composition for predominant cations and anions, they are of the sodium chloride type.

Table 1. Statistical parameters of the chemical data of the Li-bearing brines of Guaranda.

Element	Min ¹	Max	Mean	Median	S.D.
Ca (mg/L)	747.35	1266.28	998.72	987.78	186.54
K	1977.25	3007.87	2507.97	2517.12	338.56
Mg	460.82	525.13	485.78	475.61	22.49
Na	17516.34	21710.01	19192.80	18912.88	1463.95
Zn	0.25	3.56	1.25	0.62	1.39
Pb	0.27	0.68	0.39	0.31	0.18
Cd	0.10	1.08	0.31	0.19	0.32
Ba	0.02	0.04	0.03	0.03	0.01
Fe	0.25	41.47	8.77	4.46	13.48
Mn	0.12	1.83	0.94	0.97	0.54
Li	203.25	268.73	226.38	222.46	22.80
Rb	20.92	31.15	25.02	24.24	3.50
Se	0.13	0.28	0.18	0.16	0.05
Be	0.15	0.17	0.16	0.16	0.01
Sr	4.97	6.03	5.35	5.28	0.33
Cl ⁻	28308	52080	40891	41710	9216
CO ₃ ²⁻	3	5	4	4	2
HCO ₃ ⁻	478	781	549	494	119
SO ₄ ²⁻	1263	1951	1663	1738	296

¹Min, Max, Mean, Median, Standard Deviation in mg/L (ppm).

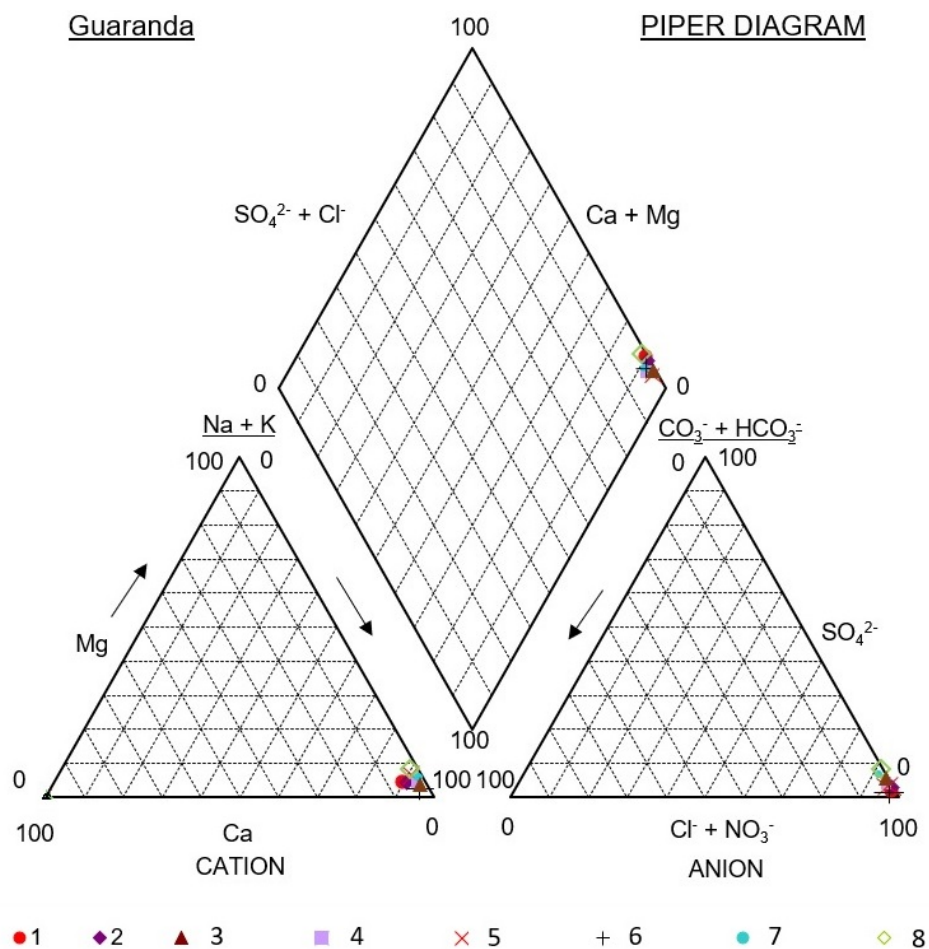


Figure 4. Piper diagram of Li-bearing brines samples.

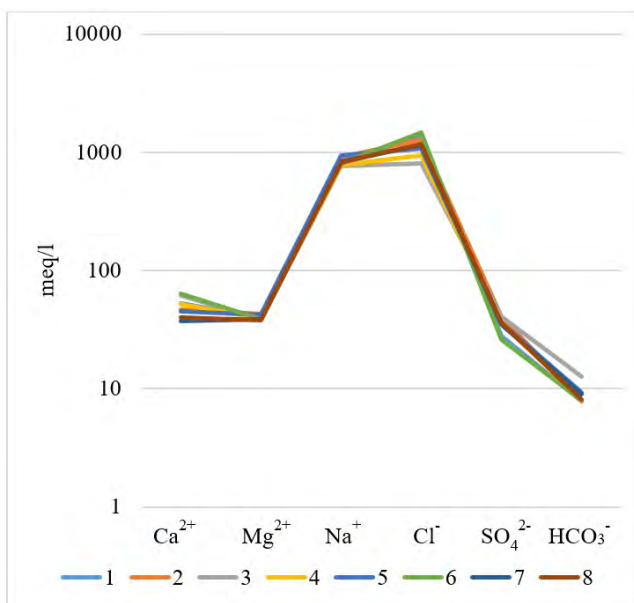


Figure 5. Schöeller-Berkaloff diagram of Li-bearing brines samples.

Li-bearing solids of the Guaranda

The statistical treatments of the chemical data of the Li-bearing solids of Guaranda are given in Table 2. Contents of Be, Li, and reached sub-anomalies

values (median + 2 standard deviation) (Howarth, 1983), whereas sub-anomalies or anomalies of other trace elements, such as Ba, Mn, Rb and, Sr, were not detected (Table 3).

Table 2. Statistical parameters of the chemical data of the Li-bearing solids of Guaranda.

Element	Min ¹	Max	Mean	Median	S.D.
SiO ₂ (wt%)	1.57	63.26	22.41	4.76	27.17
Al ₂ O ₃	0.16	7.20	2.98	2.80	2.51
CaO	0.24	68.50	30.79	20.82	26.76
MgO	0.12	11.30	1.69	0.25	3.89
K ₂ O	0.02	10.49	3.92	3.72	3.83
P ₂ O ₅	0.74	2.78	1.72	1.72	0.57
S	0.94	14.43	2.79	1.16	4.70
Na ₂ O	3.37	32.31	7.37	3.89	10.08
Fe ₂ O ₃	0.02	8.38	2.12	0.30	3.25
Ba (ppm)	3.9	33.6	25.7	29.1	9.5
Be	3.9	5.0	4.2	4.1	0.3
Mn	4.3	610.6	276.3	261.6	178.8
Li	128.0	1109.4	312.0	201.5	326.2
Rb	62.5	312.9	213.0	217.5	76.5
Sr	127.0	215.0	192.8	198.8	28.0

¹Min, Max, Mean, Median, Standard Deviation in wt% (SiO₂ to Fe₂O₃) and ppm (Ba and below).

Table 3. Geochemical anomalies of the Li-bearing solids of Guaranda.

Element	Background	Threshold	Sub anomaly
SiO ₂ (wt%)	4.76	31.93	59.09
Al ₂ O ₃	2.80	5.31	
CaO	20.82	47.57	
MgO	0.25	4.14	8.03
K ₂ O	3.72	7.55	
P ₂ O ₅	1.72	2.29	
S	1.16	5.86	10.57
Na ₂ O	3.89	13.98	24.06
Fe ₂ O ₃	0.30	3.55	6.81
Ba (ppm)	29.1		
Be	4.1	4.5	4.8
Mn	261.6	440.4	
Li	201.5	527.7	853.8
Rb	217.5	294.1	
Sr	198.8		

SiO₂ to Fe₂O₃ in wt% and ppm (Ba and below). Background was calculated with the median of data, threshold (median + stand dev) and sub anomaly (median + 2*stand dev). Anomalies were not detected.

The mineralogical analyzes carried out by X-ray diffraction (XRD) have revealed that the solids are composed predominantly of calcite (CaCO₃) and halite (NaCl) (Table 4). In addition, saponite and fluor-

ferroleakeite as lithium-bearing minerals (likely), as well as silicates, clays, sulfates, halides, borates, phosphates and nitrates have been identified.

Table 4. XRD mineralogy of the solid samples from Guaranda.

Sample ID	Major ¹	Moderate	Minor
1	Halite	Saponite ²	Gypsum, Sylvite
2	Calcite	---	Mutinaite, Brushite, Halite
3	Calcite	---	Halite
4	Quartz	Calcite, Orthoclase, Mutinaite, Sylvite	Fluor-ferroleakeite ² , Halite
5	Orthoclase, Quartz	Fluor-ferroleakeite ² , Halite, Calcite	Halite
6	Calcite	---	---
7	Calcite	Quartz, Fluor-ferroleakeite ² , Orthoclase, Mutinaite, Brushite, Sylvite,	Halite
8	Gypsum	---	Nitre

¹Major >25%; Moderate 5%–25%; Minor <5%; ²Saponite and fluor-ferroleakeite as lithium-bearing minerals (likely).

Discussion

Li-bearing hydrothermal brines of the Guaranda

The major chemical composition of the studied brines is rather constant; brines are typically rich in Na⁺ and Cl⁻, subordinated SO₄²⁻, and relatively poor in Ca²⁺, Mg²⁺ and HCO₃⁻ + CO₃²⁻. Another fact is that in the Guaranda brines the concentrations of K⁺ are 4 to 6 times higher than those of Mg²⁺.

The low Ca²⁺ concentrations observed at Guaranda (median 987.78 mg/L, Table 1) may be determined by contributions from freshwater (meteoric) (Inguaggiato *et al.*, 2010) with depleted Ca²⁺ concentrations and/or the precipitation of calcite, may be the result of the local geochemical processes that cause it-, which is one of the main mineral phases identified in the crusts around the upwelling pools, which is reported as travertine (BGS-CODIGEM, 1997). Lower concentrations of dissolved carbon (HCO₃⁻ + CO₃²⁻) have been measured in these hot springs and

the presence of travertine deposits in this region is evident, which could be since that carbon is eliminated by kinetic fractionation, through precipitation of carbonate.

This chemical composition is controlled by limited concentrations of carbonate and Ca²⁺ resulting in relatively richer sulfate, chloride and sodium content at increasing stages of evaporation, which is typical of mature brine in equilibrium with water halite (NaCl) and mirabilite (Na₂SO₄) (Hardie and Eugster, 1970), although the latter was not detected in the present study.

The ratio Na⁺:Cl⁻ (1:0.7) indicates the precipitation of halite. The negative trend between Ca²⁺:Cl⁻ (Figure 6) indicates the precipitation of calcite before halite, due to the difference in the solubilities of these mineral phases. In addition, the Ca negative deviation represents the local removal of cations by adsorption or ion exchange (Schijf, 2007).

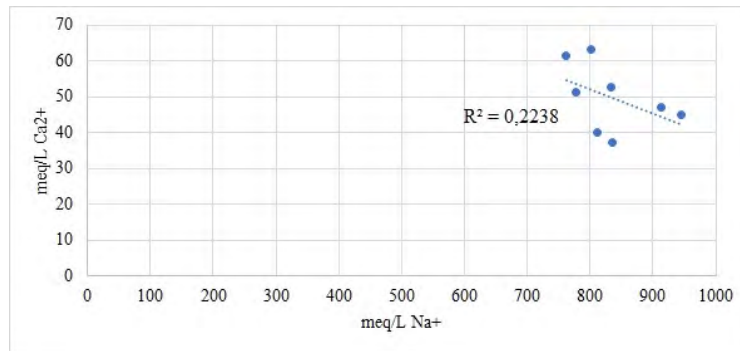


Figure 6. Scatter diagram Na⁺ vs Ca²⁺.

The Li⁺ concentration in brines ranges from 203.25 to 268.73 mg/L in Guaranda. The Li:Mg median ratios are 0.82, while the mean Li:K median ratios is 0.51, in Guaranda brines. This may also suggest a common supply for most of these ions and similar geochemical behavior.

Li preferentially exists in solution and concentrates in clays (saponites) after long cycles of water evaporation and precipitation of soluble, non-Li salts (eg, halite or calcite). This is supported by the lack of correlation between Li and major ions such as Cl⁻ and Na⁺ (López-Steinmetz *et al.*, 2020).

Li-bearing salts and crust of the Guaranda

Mineralogical analysis by XRD, determined that most of the samples contain calcite, except for of sample 1 which is composed mainly of halite and saponite, and sample 8 which is composed mainly of gypsum and niter. Clay from the hectorite group, saponite, was detected in sample 1, which contains the highest concentration of Li in the study. In three samples, fluoroferroleakeite was detected, which is a sodium amphibole with Li on structure lattice (Na₃Fe²⁺₂Fe³⁺₂Li(Si₈O₂₂)F₂),

which can be found in mildly peralkaline porphyry (Hawthorne *et al.*, 2001). Additionally other mineral phases were identified as quartz, orthoclase, sylvite, brushite and mutinaite, in general silicates, chlorides and phosphates.

With the data on the chemical composition of the Guaranda solids, a multivariate statistical analysis was made. In the principal component analysis (Figure 7), it is shown that Li is associated with Be and Na, which indicates a geochemical association between elements in clays (saponite) and in halite, where Li⁺ and Be²⁺ can replace Mg²⁺ (Misra, 2012), mainly in saponite, since the replacement of Li⁺ for Na⁺ in halite may be more limited, due to differences in ionic radius While Mg, Ca, S, P, Ba and Sr, can be associated, which corresponds to, calcite, gypsum and brushite, in which trace elements such as Ba and Sr can be in the lattice structures of these mineral phases, for if the similarity in ionic potential with major and minor elements such as Ca and Mg. Another specific geochemical association is that of Si, K, Al, Fe, Mn, and Rb, which indicates the silicate and clay phases, in which Rb⁺ for example could replace K⁺.

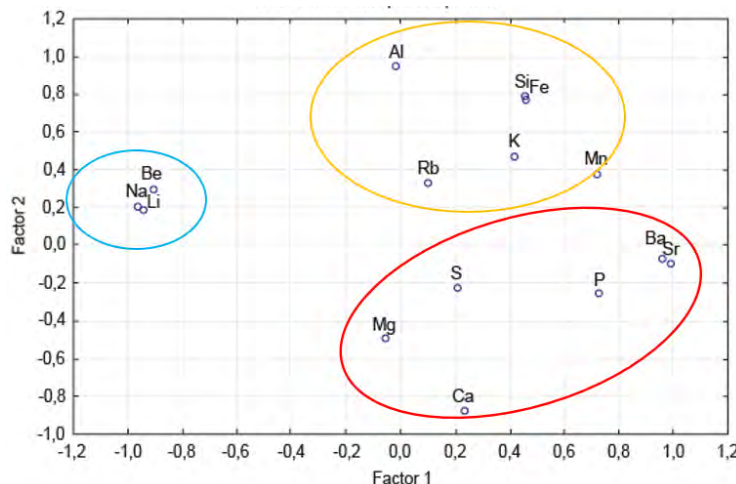


Figure 7. Factorial plot, Factor 1 vs. Factor 2

These geochemical associations are also shown in the factor analysis (Table 5). Na (-0.964), Be (-0.908) and Li (-0.945) are grouped into factor 1, indicating a similar geochemical behavior of these elements, and on the other hand P (0.724), Ba (0.957), Sr (0.985), related to phosphates, carbonates and sulfates. In factor 2, Si (0.799), Al (0.955), and Fe (0.778) are grouped, which would correspond to silicates and aluminosilicates, in addition to that factor, Ca shows an inverse behavior (-0.868), associated with carbonates, sulfates and phosphates with Mg, P, S, Ba and Sr.

Table 5. Factor loadings (unrotated) of chemical compositions Guaranda's solids.

Variable	Factor 1	Factor 2
Si	0.455124	0.799416
Al	-0.015973	0.955667
Ca	0.231243	-0.868765
Mg	-0.055467	-0.483292
K	0.415438	0.475070
P	0.724530	-0.249845
S	0.203776	-0.218279
Na	-0.964237	0.211874
Fe	0.459412	0.778542
Ba	0.957046	-0.065785
Be	-0.908349	0.296302
Mn	0.714529	0.381151
Li	-0.945980	0.194031
Rb	0.102327	0.336380
Sr	0.985293	-0.092183

Lithium also constitutes part of the lattice structure in the clays (hectorites) of the Clayton Valley (230 ppm Li), USA, for example, which host the lithium brines in what is now a shuttered brine plant (Davis *et al.*, 1986; Warren, 2014). In the mineralogical analyzes, the saponite ($\text{Ca}_{0.1}\text{Na}_{0.1}\text{Mg}_{2.25}\text{Fe}^{2+}_{0.75}\text{Si}_3\text{AlO}_{10}(\text{OH})_2 \cdot 4(\text{H}_2\text{O})$) clay was identified in sample 1, which presents the highest concentration of Li detected in the study, 1109.4 ppm. This mineral phase belongs to the group of hectorite (smectite group), which is a clay of hydrothermal/volcanic origin in whose lattice structure Li^+ (0.60 Å) can replace Mg^{2+} (0.65 Å) (Railsback, 2003).

The high Li content (average 201.5 ppm) in Guaranda solids may be of interest, as economical deposits of lithium carbonate and borate salts tend to form in non-marine environments and are common in high-altitude depressions, especially in subduction-related orogenic belts and other fault zones in the Earth's continental

crust (Ozol, 1978; Garrett, 2004; Warren, 2014). The hydrothermal brine upwelling pools are located at 3550 m a.s.l. altitude, in a volcanic geological terrain, constituted by the Zumbagua Group, in the subduction zone of the Nazca plate with the South American plate, resembling other Li-bearing brine deposits mentioned by Warren (2014).

Probably higher altitude, active tectonism/continental vulcanism, hydrothermal fluids and cooler climate are significant factors that are controlling the mobility and geochemical concentration of Li occurrences in the brines of Guaranda, Ecuador.

Conclusions

Brines sampled in the Salinas de Guaranda sector are of the sodium chloride type, which produces the precipitation of halite by evaporation.

The geochemical composition of the sampled hydrothermal fluids is the result of strong water-rock interactions associated with active hydrothermal volcanic fluids and/or surface water recharge, resulting in mineral dissolution.

Sub-anomalies values of Li (222.46 mgL^{-1} median) in brines and Li in Guaranda solids (201.5 mgL^{-1} median), can be comparable to exploitable Li deposits worldwide, which is interesting for its possible economic use.

Based on the multivariate statistical analysis, the chemical and mineralogical results, Li is associated with Be, Na, in the solids analyzed, this is evidenced in the detection of saponite and fluoro-ferroleakeite.

A second geochemical association was determined in the study with Ca, Mg, S, P, Ba and, Sr, related to carbonates (calcite or travertine), sulphates (gypsum) and phosphates (brushite). Finally, a third geochemical association with silicates and aluminosilicates containing: Si, Al, K, Fe, Mn and, Rb.

Acknowledgments

This study was funded by the Innovation Project Code: PROY_INNOV_INGC_2019_2605, of the Universidad Técnica Particular de Loja. We thank the Vice-Rectorate for Research, Prendho UTPL and the Department of Geosciences for their logistical and financial support.

References

- Andreu, J.M.; Calaforra, J.M.; Cañaveras, J.C.; Cuezva, S.; Durán, J.J.; Garay, P.; García del Cura, M.A.; García-Cortés, A.; Gázquez, F.; Ordóñez, S.; Sánchez-Moral, S. (2016). Karst: un concepto muy diverso. *Enseñanza de las Ciencias de la Tierra*, 24(1), 6-20.
- BGS-CODIGEM. (1997). Mapa geológico de la Cordillera Occidental del Ecuador entre 1°-2° S. Dirección Nacional de Geología, Quito, Ecuador, escala 1:200000.
- Changes, A.; Swiatowska, J. (2015). *Lithium Process Chemistry: Resources, Extraction, Batteries, and Recycling*. Elsevier.
- Davis, J.R.; Friedman, I.; Gleason, J.D. (1986). Origin of the lithium-rich brine, Clayton Valley, Nevada. *US Geological Survey Bulletin*, 1622, 131-138.
- Dill, H. (2010). The “chessboard” classification scheme of mineral deposits: Mineralogy and geology from aluminum to zirconium. *Earth-Science Reviews*, 100(1-4), 1-420. <https://doi.org/10.1016/j.earscirev.2009.10.011>
- Garrett, D.E. (2004). *Handbook of Lithium and Natural Calcium Chloride: Their Deposits, Processing, Uses and Properties*. Elsevier Academic Press.
- Gonzaga, M.; Eguez, A.; Villares, F.; Cerón, G. (2017). Evaluación geoestadística del potencial de litio en la Cordillera Occidental del Ecuador. *VIII. Jornadas Ciencias de la Tierra*, Quito, Ecuador.
- Hardie, L.; Eugster, H. (1970). The evolution of closed-basin brines. *Mineralogical Society of America Special Publication*, 3, 273-290.
- Howarth, R.J. (1983). *Statistics and Data Analysis in Geochemical Prospecting*. Handbook of Geochemical Exploration, Vol. 2. Elsevier.
- Hawthorne, F.; Oberti, R.; Canillo, E.; Ottolini, L.; Roelofsen, J.N.; Martin, R.F. (2001). Li-bearing arfvedsonitic amphiboles from the Strange Lake peralkaline granite, Quebec. *The Canadian Mineralogist*, 39(4), 1161-1170. <https://doi.org/10.2113/gscanmin.39.4.1161>
- Inguaggiato, S.; Hidalgo, S.; Beate, B.; Bourquin, J. (2010). Geochemical and isotopic characterization of volcanic and geothermal fluids discharged from the Ecuadorian volcanic arc. *Geofluids*, 10(4), 525-541. <https://doi.org/10.1111/j.1468-8123.2010.00315.x>
- Li, Y.H. (1982). A brief discussion on the mean oceanic residence time of elements. *Geochimica et Cosmochimica Acta*, 46(12), 2671-2675. [https://doi.org/10.1016/0016-7037\(82\)90386-6](https://doi.org/10.1016/0016-7037(82)90386-6)
- López-Steinmetz, R.L.; Salvi, S.; Sarchi, C.; Santamans, C.; López-Steinmetz, L.C. (2020). Lithium and Brine Geochemistry in the Salars of the Southern Puna, Andean Plateau of Argentina. *Economic Geology*, 115(5), 1079-1096. <https://doi.org/10.5382/econgeo.4754>
- Misra, K. (2012). *Introduction to Geochemistry Principles and Applications*. Wiley-Blackwell.
- Munk, L.; Hynek, S.; Bradley, D.; Boutt, D.; Labay, K.; Jochens, H. (2016). Lithium Brines: A Global Perspective. *Reviews in Economic Geology*, 18, 339-365. <https://doi.org/10.5382/Rev.18.14>
- Ozol, A. (1978). Plate tectonics and the process of volcanogenic-sedimentary formation of boron. *International Geology Review*, 20(6), 692-698. <https://doi.org/10.1080/00206817809471439>
- Pohl, W. (2011). *Economic Geology Principles and Practice Metals, Minerals, Coal and Hydrocarbons – Introduction to Formation and Sustainable Exploitation of Mineral Deposits*. John Wiley & Sons Ltd. <https://doi.org/10.1002/9781444394870>
- Railsback, L. (2003). An earth scientist's periodic table of the elements and their ions. *Geology*, 31(9), 737-740. <https://doi.org/10.1130/G19542.1>
- Schijf, J. (2007). Alkali elements (Na, K, Rb) and alkaline earth elements (Mg, Ca, Sr, Ba) in the anoxic brine of Orca Basin, northern Gulf of Mexico. *Chemical Geology*, 243(3-4), 255-274. <https://doi.org/10.1016/j.chemgeo.2007.06.011>
- USGS (2022). *Mineral commodity summaries 2022*. U. S. Geological Survey.
- Warren, J. (2014). Geochemistry of Evaporite Ores in an Earth-Scale Climatic and Tectonic Framework. In: K. Turekina, H. Holland (ed.). *Treatise on Geochemistry* (pp. 569-593). 2nd Edition. Vol. 13. Elsevier. <https://doi.org/10.1016/B978-0-08-095975-7.01125-6>
- Webmineral. (2022). Hectorite. <https://www.webmineral.com/data/Hectorite.shtml>

Received: 01 June 2022

Accepted: 23 March 2023

Supplementary Table 1. Liquid sample chemistry data and coordinates.

Sample	Coordinates X	Coordinates Y	Analyte Symbol	Ca	K	Mg	Na	Zn	Pb	Cd	Ba	Fe	Mn	Li	Rb	As	Se	Be	Sr		
			Unit Symbol	(mg/L)	(mg/L)	(mg/L)	(mg/L)	(mg/L)	(mg/L)	(mg/L)	(mg/L)	(mg/L)	(mg/L)	(mg/L)	(mg/L)	(mg/L)	(mg/L)	(mg/L)	(mg/L)	(mg/L)	(mg/L)
			Detection Limit	0.01	0.01	0.01	0.01	0.01	0.01	0.01	0.01	0.01	0.01	0.01	0.01	0.01	0.01	0.01	0.01	0.01	0.01
			Analysis Method	ICP- OES	ICP- OES	ICP- OES	ICP-OES	ICP- OES	ICP- OES	ICP- OES	ICP- OES	ICP- OES	ICP- OES	ICP- OES	ICP- OES	ICP- OES	ICP- OES	ICP- OES	ICP- OES	ICP- OES	ICP- OES
1	720332	9844325		1057.02	2549.87	489.27	19150.25	3.40	0.68	0.22	0.03	5.34	1.09	268.73	22.22	12.22	0.22	0.17	4.97		
2	720332	9844325		942.90	3007.87	525.13	20985.16	3.56	0.68	0.24	0.03	4.56	1.01	237.72	20.92	1.20	0.20	0.17	6.03		
3	720332	9844325		1233.87	2484.37	474.36	17516.34	0.87	0.31	0.17	0.03	2.99	0.66	242.41	23.76	1.70	0.16	0.16	5.33		
4	720313	9844336		1032.66	2640.79	476.87	17864.96	0.49	0.27	0.42	0.03	9.21	1.47	203.25	22.39	5.89	0.15	0.16	5.19		
5	720313	9844336		901.91	2872.83	514.21	21710.01	0.37	0.27	0.17	0.03	4.36	0.92	214.07	26.34	4.35	0.13	0.15	5.10		
6	720313	9844336		1266.28	2262.82	473.91	18412.55	0.34	0.27	0.12	0.02	1.95	0.46	206.10	24.72	4.22	0.13	0.16	5.47		
7	720285	9844335		747.35	2267.95	471.69	19227.59	0.76	0.31	1.08	0.04	41.47	1.83	207.90	31.15	38.90	0.15	0.17	5.23		
8	720285	9844335		807.76	1977.25	460.82	18675.51	0.25	0.31	0.10	0.02	0.25	0.12	230.85	28.65	3.19	0.28	0.17	5.50		

Supplementary Table 2. Solid sample chemistry data and coordinates.

Sample	Coordinates X	Coordinates Y	Analyte Symbol	SiO ₂	Al ₂ O ₃	CaO	MgO	K ₂ O	P ₂ O ₅	S	Na ₂ O	Fe ₂ O ₃	LOI	Ba	Be	Mn	Li	Rb	Sr		
			Unit Symbol	wt. %	wt. %	wt. %	wt. %	wt. %	wt. %	wt. %	wt. %	wt. %	wt. %	wt. %	(mg/Kg)	(mg/Kg)	(mg/Kg)	(mg/Kg)	(mg/Kg)	(mg/Kg)	
			Detection Limit	0.01	0.01	0.01	0.01	0.01	0.01	0.01	0.01	0.01	0.01	0.01	0.01	0.1	0.1	0.1	0.1	0.1	0.1
			Analysis Method	XRF	XRF	XRF	XRF	XRF	XRF	XRF	XRF	XRF	ICP-OES	XRF		ICP-OES	ICP-OES	ICP-OES	ICP-OES	ICP-OES	ICP-OES
1	720332	9844325		2.60	3.05	0.24	0.89	1.83	0.74	0.97	32.31	0.02	57.35	3.9	5.0	4.3	1109.4	186.0	127.0		
2	720332	9844325		5.66	0.16	61.90	0.33	0.02	1.68	1.27	3.88	0.29	24.81	25.3	3.9	164.1	206.1	286.8	191.3		
3	720332	9844325		3.86	<0.01	68.50	11.30	0.39	1.98	1.40	4.18	0.18	8.22	22.4	4.2	260.1	172.0	239.4	195.1		
4 (S9.4)	720313	9844336		55.70	2.80	14.49	0.23	6.04	1.75	0.94	3.37	1.47	13.22	30.0	4.1	263.1	209.3	232.4	193.1		
5	720313	9844336		63.26	7.20	5.47	0.12	6.65	1.39	1.05	3.91	8.38	2.58	28.4	4.2	610.6	128.0	312.9	207.2		
6	720313	9844336		1.66	<0.01	54.10	0.19	0.37	1.69	1.31	3.67	0.30	36.71	32.1	4.1	278.0	196.9	181.3	202.5		
7 (S9.7)	720285	9844335		44.94	1.71	16.40	0.27	5.62	2.78	0.98	4.04	6.11	17.15	33.6	4.1	210.0	304.6	202.7	215.0		
8	720285	9844335		1.57	<0.01	25.24	0.16	10.49	1.79	14.43	3.58	0.17	42.57	29.9	4.2	419.9	169.5	62.5	211.5		

Continuation Supplementary Table 2.

Sample	Coordinates X	Coordinates Y
ActLabs		
Report Number: A20-10861		
Report Date: 30/9/2020		
Analyte Symbol	Li	Li ₂ O
Unit Symbol	%	%
Detection Limit	0.01	0.01
Analysis Method	FUS-Na ₂ O ₂	FUS-Na ₂ O ₂
S9.4	0.02	0.04
S9.7	0.03	0.06
QC		
NCS DC86303 Meas	0.22	0.47
NCS DC86303 Cert	0.21	0.46
NCS DC86303 Meas		
NCS DC86303 Cert		
NCS DC86304 Meas	1.1	2.36
NCS DC86304 Cert	1.06	2.29
NCS DC86314 Meas	1.86	4.01
NCS DC86314 Cert	1.81	3.89
CZN-4 Meas		
CZN-4 Cert		
Lithium Tetraborate FX-LT 100 lot#220610B Meas	8.62	
Lithium Tetraborate FX-LT 100 lot#220610B Cert	8	
Lithium Tetraborate FX-LT 100 lot#220610B Meas	7.8	
Lithium Tetraborate FX-LT 100 lot#220610B Cert	8	
S9.7 Orig	0.03	0.06
S9.7 Dup	0.03	0.06
Method Blank	< 0.01	< 0.01